JOURNAL OF AIRCRAFT
Vol. 42, No. 1, January–February 2005

Five-Hole Flow Angle Probe Calibration from Dynamic and Tower Flyby Maneuvers

V. Parameswaran*
National Aerospace Laboratories, Bangalore 560 017, India
and
R. V. Jategaonkar† and M. Press‡
DLR, German Aerospace Center, 38108 Brunswick, Germany

Flight-test and data analysis techniques applied to calibrate the static pressure measured by pitot static systems and the flow angles measured by a five-hole probe mounted on a noseboom are described. Dynamic maneuvers with rapid variations in the aircraft motion are analyzed by application of parameter estimation techniques based on the output error method to calibrate the angle of attack and angle of sideslip. A complementary approach based on the Kalman filter technique is applied to a wind-box maneuver to calibrate the flow variables. The tower flyby maneuvers are analyzed using the classical approach of altitude determination through geometrical evaluation of photographs, and accurate information is derived from redundant sources to calibrate the pitot static system. The investigations showed that the static pressure measured by aircraft-installed pitot static system is accurate, sufficiently whereas that measured by an additional sensor mounted on the noseboom required speed-dependent correction. The flight estimated sensitivity factors for the flow angles measured by the five-hole probe agreed reasonably well with the manufacturer's specifications subject to corrections for biases resulting from misalignment and time delays caused by the recording equipment.

Introduction

ACCURATE knowledge about the flow angles, that is, angle of attack and angle of sideslip, is necessary for many applications, for example, in-flight simulation and model-following control. Conventionally, the flow angles are measured using vanes mounted either on the fuselage or on the noseboom. In the case of the Advanced Technologies Testing Aircraft System (ATTAS), a test bed for in-flight simulation at the DLR, German Aerospace Center, a flight log mounted on the noseboom was hitherto used for this purpose.[1−3] It is known that the dynamics of the vane influences the measurements of flow angles. Moreover, vanes have mechanical difficulties, such as friction and grit in the bearings, and are prone to malfunctioning as well as damage in bad weather conditions. To overcome these limitations, a flight log with vanes has been replaced by a fast response five-hole probe, which is more robust, reliable, and suitable for operation in adverse weather conditions. The main goal of the investigations reported in this paper is to calibrate accurately the five-hole probe, that is, to obtain accurate flow angles from the measured total and difference pressures. In the sequel, it is also necessary to calibrate the static pressure source at the noseboom.

For the specific purpose of calibrating the five-hole probe, a comprehensive flight-test program was carried out with ATTAS (Fig. 1). A total of four flights were flown, covering four flap positions and the complete range of Mach numbers. The flight tests consisted of 1) dynamic maneuvers with rapid variations in pitch and yaw axes, 2) steady-state sideslip maneuvers, 3) wind-box maneuvers eliminating the spatial, X–Y plane, wind effects for flow angle calibration and 4) tower flyby tests for calibration of the static pressure ports.

Presented as Paper 2002-4627 at the AIAA Atmospheric Flight Mechanics Conference, Monterey, CA, 5 August 2002; received 9 October 2003; revision received 5 December 2003; accepted for publication 6 December 2003.

*Scientist, Flight Mechanics and Control Division, P.O. Box 1779.
†Senior Scientist, Institute of Flight Research, Lilienthalplatz 7. Associate Fellow AIAA.
‡Flight Test Engineer, Flight Operations.

A flight-path reconstruction technique[2,4,5] and parameter estimation methods[6−8] are applied to analyze the flight maneuvers and to calibrate angle of attack and angle of sideslip. Additionally, the calibration of static pressure measurements from tower flyby tests through photograph evaluation techniques is elaborated.

Position Error in Static Pressure

Deriving airspeed and altitude information from total and static pressures needs accurate measurements of these pressures in freestream air. Besides indirectly influencing the other measured or computed variables, accurate static pressure information is also necessary for vertical spacing, that is, for safety reasons. Generally, the static pressure measured by the pitot static system mounted on an aircraft in flight differs from freestream pressure.[9,10] This difference is primarily dependent on the location of the pressure ports, the speed and the altitude; secondary effects due to angle of attack and Reynold's number may also exist. Because the static pressure field varies along the length of an aircraft, it is necessary to choose appropriately the location of the ports mounted on the fuselage (Fig. 2, source Ref. 9) showing the measured pressure minus the true static pressure, ΔP, normalized to compressible dynamic pressure q_c, plotted as a function of fuselage position. In the case of ports mounted on a noseboom, the length of the boom, which may be limited due to other considerations such weight, structural vibrations, and stability, is an important criterion.

The commonly adopted procedures to calibrate the static pressure ports are 1) trailing cone and 2) tower flyby.[11] The trailing cone procedure compares the static pressure measured by aircraft's pitot static system to the freestream static pressure measured behind the aircraft by a static source. A long tube is necessary to sense the ambient pressure out of the aircraft's wake. The cone helps to stabilize the tube and to keep it taut. The overall procedure is somewhat difficult in practice, requires very accurate and steady flight, and is associated with some risk resulting from instabilities, which are difficult to predict. On the other hand, the tower flyby method is a simpler procedure to calibrate accurately the static pressure measurements. The test procedure consists of flying the aircraft past an observation tower and recording the geometrical position of the aircraft, for example, using a camera. The second approach, namely, tower flyby, is adopted in this investigation.

Table 1 Test flight conditions

Flaps, deg	KIAS											
	120	130	140	145	150	160	170	180	190	200	210	240
14	×		×			×			×			
5		×			×			×			×	
1			×				×			×		×
Clean(−6)				×			×			×		×

Fig. 1 Test aircraft ATTAS with five-hole probe.

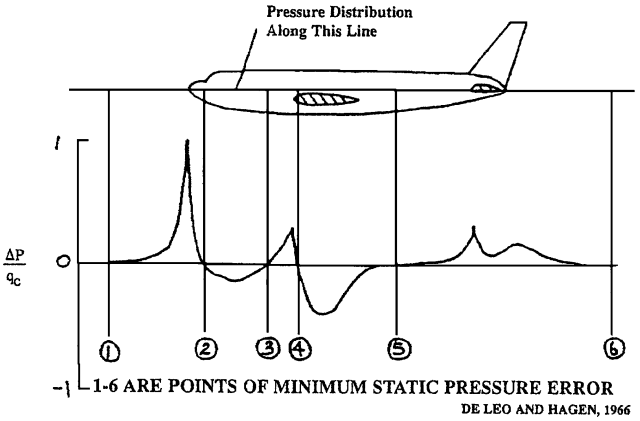

Fig. 2 Static pressure field along the length of aircraft.

Tower Flyby and Measurements

The tower flyby tests were performed at four flap positions covering the speed range from 120 to 240 knots indicated airspeed (KIAS) (Mach number roughly 0.14–0.45). Table 1 defines the flight-test matrix of airspeed and flap setting. At each flight condition a tower flyby is performed, while the height above the runway and the speed are kept constant as far as possible. The nominal height above the runway is about 150 ft.

An onboard measurement system installed in the test aircraft ATTAS provides measurements of a large number of signals such as aircraft motion variables, atmospheric conditions, control surface positions, engine parameters, etc. Pertinent to the current aspect of investigations, the onboard measurements of altitude, static pressure, total pressure, and temperature are obtained from the digital air data computer (DADC). The altitude above ground Level (AGL), that is the runway, is measured using the radio altimeter.

Besides the cited standard onboard measurements, the position of the aircraft above the runway during the flyby is photographed, as well as filmed by a digital video camera from the top of the observation tower. The static pressure and temperature are recorded at the observation tower. Furthermore, the QNH, that is, actual air pressure calculated to mean sea level, relayed by the control tower, is recorded.

Data Analysis

A schematic of the tower flyby maneuver analysis is shown in Fig. 3. When the tower height and distance from tower to runway centerline and to marking lights are known, it is a simple geometrical procedure to evaluate the photographs to obtain the height above the runway. After the AGL is determined, it is straightforward to obtain the aircraft altitude above sea level from the known flat runway elevation. Figure 4 provides the altitude above sea level as obtained from the geometrically computed height above runway from the two different cameras. Some small differences are observed in the altitudes obtained from the two cameras. These minor deviations are attributed mostly to the variations in the flight path above the runway, different time points of exposure, and manual evaluation procedure. Nevertheless, these altitudes, obtained from two independent sources, match fairly well with the radio altitude. The same approach can be applied to the information that is usually available from global positioning system (GPS); in the present case, however, due to malfunctioning of the GPS receiver, the photographic technique, which is the classical approach, was adopted and also provided redundant measurements.

From the measured pressure altitude h during the tower flyby, the static pressure p_{st} is obtained as

$$p_{st} = p_{0\,act}[1 - (0.0065/T_{0\,act})h]^{5.25588} \tag{1}$$

where $p_{0\,act}$ and T_{0act} are the current QNH and temperature at the time of the particular test. The temperature gradient of 0.0065°K/m is assumed according to the standard atmosphere specifications; $p_{0\,act}$ and $T_{0\,act}$ are noted during each tower flyby.

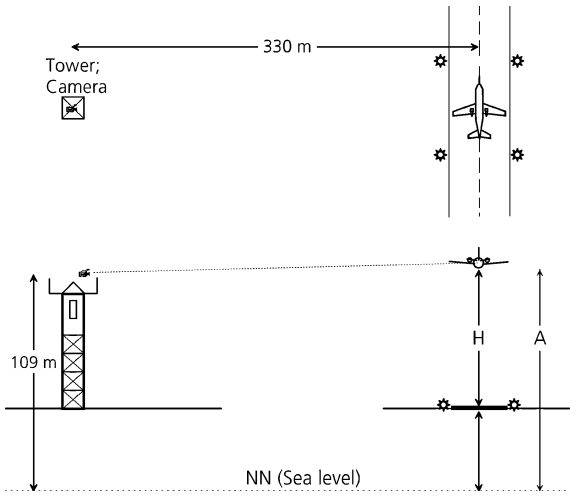

Fig. 3 Schematic of tower flyby maneuver analysis.

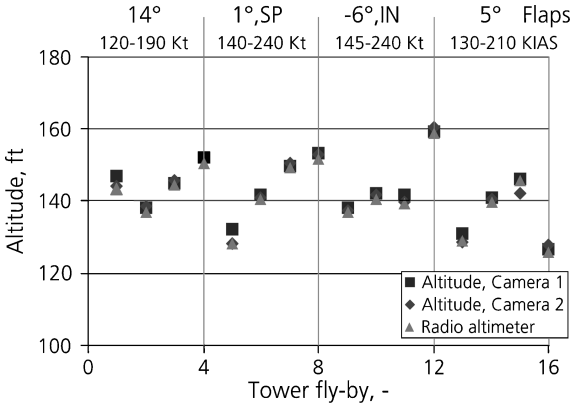

Fig. 4 Altitude above runway during tower flyby.

In the present investigations, it was noted that the variations in $T_{0\,\mathrm{act}}$ during the complete flight test were less than 0.5°C and, hence, were neglected in the detailed computation of static pressure for each flyby. The average temperature was 18°C. The static pressure at sea level at takeoff was 1013 hPa. For most of the flight maneuvers, which lasted 1 h 40 min, it was 1012 hPa.

Based on the earlier noted $T_{0\,\mathrm{act}}$ and $p_{0\,\mathrm{act}}$, the static pressure in hectopascal at the altitude h_{rad} during each flyby is obtained from

$$p_{\mathrm{st\_rad}} = 1012\left(1 - 2.23253 \times 10^{-5} \times h_{\mathrm{rad}}\right)^{5.25588} \tag{2}$$

These static pressure values $p_{\mathrm{st\_rad}}$, which correspond to the altitude above sea level obtained from the radio altimeter measurements shown in Fig. 4, are plotted in Fig. 5.

Figure 5 also gives values of p_{st_m} and p_{stNB_m}, the static pressure measured by the basis system (DADC) and that by the five-hole probe. These mean values are obtained from the time histories for the tower flyby phase during the 16 maneuvers (not shown here). From Fig. 5, observe that, in general, the static pressure obtain by the basis system (DADC), p_{st_m}, matches well with $p_{\mathrm{st\_rad}}$, that derived from the tower flyby test evaluation. On the other hand, the static pressure values measured by the five-hole probe sensor assembly (triangles in Fig. 5) differ from the other two.

After it is concluded from Fig. 5 that the DADC and altimeter derived values are correct, the position error in the static pressure at the noseboom is the difference between p_{stNB_m} and $p_{\mathrm{st\_rad}}$. Figure 6 shows this position error in static pressure measured at the noseboom as a function of speed. For the speed range tested, the position error appears to be almost quadratic in the speed. A simple correction factor was identified from this evaluation.

In the case of ATTAS, the noseboom length was limited to roughly 1.35 times the fuselage diameter, which is probably not sufficient to reach the freestream flow, (Fig. 2). An empirical rule suggests a length of 2.5–3 times the fuselage diameter for the noseboom.[8,9]

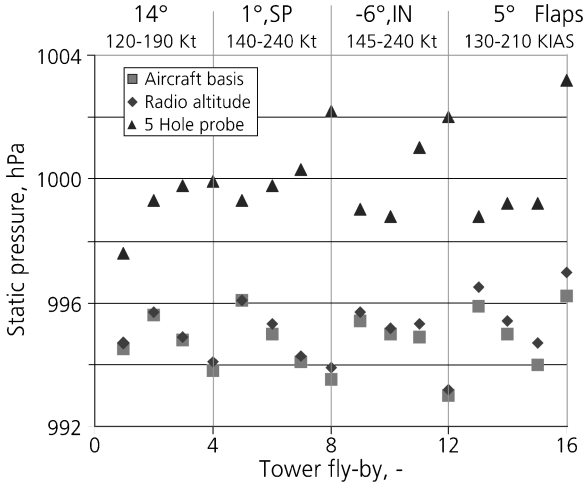

Fig. 5 Static pressures during tower flyby.

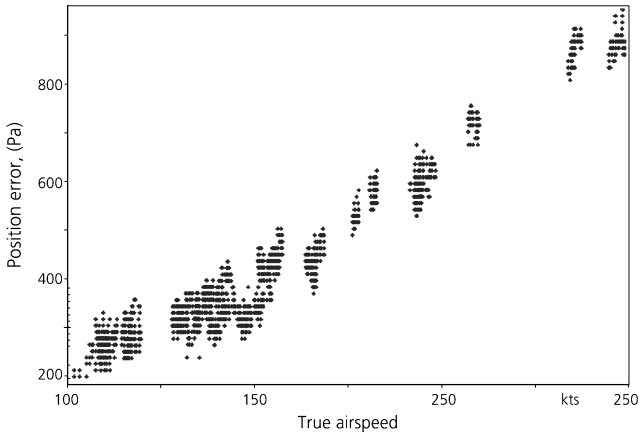

Fig. 6 Position error in static pressure measured at noseboom.

Five-Hole Probe for Flow Angles

A five-hole probe (Fig. 7) provides measurements of total pressure p_{tot}, differential pressures for angle of attack $p_{\alpha 1} - p_{\alpha 2}(= p_{d\alpha})$, and for angle of sideslip $p_{\beta 1} - p_{\beta 2}(= p_{d\beta})$. The static pressure p_{st} is also measured very close to the tip of the noseboom. The angles of attack and sideslip are then given by[12,13]

$$\alpha = \frac{p_{\alpha 1} - p_{\alpha 2}}{K p_{\mathrm{dyn}}}, \qquad \beta = \frac{p_{\beta 1} - p_{\beta 2}}{K p_{\mathrm{dyn}}} \tag{3}$$

where $p_{\mathrm{dyn}}(= p_{\mathrm{tot}} - p_{\mathrm{st}})$ is the dynamic pressure. $K = f(Ma)$ is the sensitivity coefficient specified by the manufacturer that is to be flight verified. If necessary, other corrections have to be determined.

Dynamic Maneuvers and Measurements

Flight tests were carried out in clean configuration and 14 deg flaps with gear up and nominal mid-c.g. location at flight levels of 90, 160, and 240. The trim speeds varied from 140 to 260 kn. The dynamic maneuvers consisted of a multistep elevator input to excite the short-period motion and a doublet rudder input to excite the Dutch roll. For statistical evaluation, the maneuvers were repeated at each trim condition. The amplitudes of the respective inputs were such that a variation of about ±5 deg in angle of attack and angle of sideslip was achieved. Sufficient time was allowed to damp out the resulting oscillations. In addition to the dynamic input maneuvers, steady-state sideslip and acceleration/deceleration maneuvers were performed.

As pointed out in the foregoing section, the ATTAS recording system provides measurements of a large number of signals. Relevant to the current aspect of investigation, the measurements of linear accelerations a_x, a_y, and a_z; angular rates p, q, and r, attitude angles ϕ, θ, and ψ; dynamic pressure p_{dyn}; and the difference pressures for flow angles $p_{d\alpha}$ and $p_{d\beta}$ are necessary.

Calibration of Flow Angles

Data compatibility check, sometimes called flight-path reconstruction, ensures that the measurements are consistent and error free. For example, the measured angle of attack must match with that reconstructed from the inertial measurements of accelerations and angular rates. Such a verification is possible in the case of flight data because the well-defined kinematic equations of aircraft motion provide a convenient means to bootstrap the information through a numerical procedure. Because no uncertainties are involved in the kinematic model, the compatibility check provides accurate information about the aircraft states. In addition, it provides the estimates of sensitivity factors, zero shifts, and time delays in the recorded data.[2,4,5] This approach is followed here to calibrate the angle of attack and angle of sideslip from dynamic and steady-state sideslip maneuvers. Sensitivity factors, biases, time delays, and initial conditions are estimated by application of the output error method.

Because the kinematic equations of aircraft motion are well established and can be found in any standard textbook,[14,15] they are

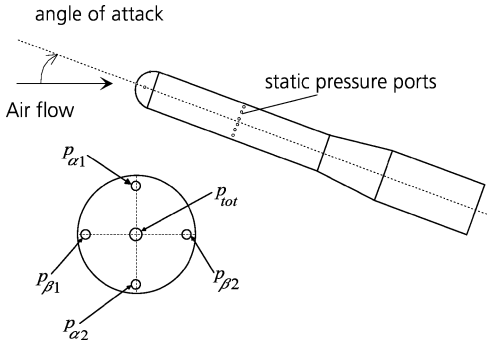

Fig. 7 Five hole probe: port configuration.

omitted here for brevity. It suffices to mention that the inputs for the flight-path reconstruction are the angular rates and linear accelerations. The state variables are the velocity components u, v, and w and attitude angles. The difference pressures for the angle of attack and angle of sideslip are modeled as

$$p_{d\alpha m} = K_\alpha p_{\text{dyn}} \alpha_{\text{nb}} + \Delta p_{d\alpha}, \qquad p_{d\beta m} = K_\beta p_{\text{dyn}} \beta_{\text{nb}} + \Delta p_{d\beta} \tag{4}$$

where K_α and K_β are the unknown sensitivity factors. Equation (4) includes bias corrections in the two difference pressure measurements. The subscript m on the left-hand side of Eq. (4) implies the measured variables. The angle of attack and angle of sideslip, α_{nb} and β_{nb}, on the right-hand side of Eq. (4) are obtained from the local velocity components that are computed from the integrated state variables by accounting for the location of the noseboom from the c.g.

To account for possible time delays resulting from the recording system, quantities on the right-hand side of Eq. (4) are appropriately modified. For example, in the case of angle of attack, the exact representation will be

$$p_{d\alpha m}(t) = K_\alpha p_{\text{dyn}}(t - \tau_{\bar{q}}) \alpha_{\text{nb}}(t - \boldsymbol{\tau}_\alpha) + \Delta p_{d\alpha} \tag{5}$$

where $\tau_{\bar{q}}$ and τ_α are the time delays in the dynamic pressure and angle of attack, respectively. They are in general not known and, hence, have to be estimated along with the unknown sensitivity factors and biases. The unknown parameter vectors thus consist of K_α, K_β, $\Delta p_{d\alpha}$, $\Delta p_{d\beta}$, $\boldsymbol{\tau}_\alpha$, $\boldsymbol{\tau}_\beta$, and $\boldsymbol{\tau}_{\bar{q}}$ and the initial conditions of the state variables and biases in the measurements of the linear accelerations. The flight tests were carried out in a steady atmospheric conditions. In cases where the turbulence level is negligible, the output error method, which accounts for measurement noise only, is found to be adequate.

Output Error Method

The output error method of parameter estimation requires model postulated in the state space,[6–8,16,17]

$$\dot{\boldsymbol{x}}(t) = \boldsymbol{f}[\boldsymbol{x}(t), \boldsymbol{X}(t,\tau), \boldsymbol{u}(t), \boldsymbol{U}(t,\tau), \boldsymbol{\Theta}] \qquad \boldsymbol{x}(t_{0,\ell}) = \boldsymbol{x}_0(b_{x,\ell}) \tag{6}$$

$$\boldsymbol{y}(t) = g[\boldsymbol{x}(t), \boldsymbol{X}(t,\tau), \boldsymbol{u}(t), \boldsymbol{U}(t,\tau), \boldsymbol{\Theta}] + \Delta \boldsymbol{z}(b_{y,\ell}), \qquad \ell = 1, \ldots, nz \tag{7}$$

$$\boldsymbol{z}(t_k) = \boldsymbol{y}(t_k) + \boldsymbol{v}(t_k), \qquad k = 1, \ldots, N \tag{8}$$

where $\boldsymbol{x}$ is the $n \times 1$ state vector, $\boldsymbol{u}$ the $p \times 1$ control input vector, $\boldsymbol{y}$ the $m \times 1$ observation (model output) vector, k is the discrete time index, and ℓ is the index for the time segment being analyzed. The n- and m-dimensional system functions $\boldsymbol{f}$ and $\boldsymbol{g}$ are general nonlinear real-valued vector functions. The measurement vector $\boldsymbol{z}$ is sampled at N discrete time points. The measurement noise vector $\boldsymbol{v}$ is assumed to be characterized by a sequence of independent Gaussian random variables with zero mean and identity covariance. The matrices $\boldsymbol{X}(t,\tau)$ and $\boldsymbol{U}(t,\tau)$ denote the time-delayed state and input variables with[17]

$$[\boldsymbol{X}(t,\tau)]_{ij} = \boldsymbol{x}_i(t - \tau_j), \qquad [\boldsymbol{U}(t,\tau)]_{ij} = \boldsymbol{u}_i(t - \tau_j) \tag{9}$$

The postulated model includes nz time records to be analyzed simultaneously. Furthermore, $\boldsymbol{\Theta}$ represents the unknown parameters, τ the unknown time delays, $\boldsymbol{x}_0$ the unknown initial conditions, and Δz the zero shifts, that is, biases, in the measurements.

The maximum likelihood estimates of unknown parameters are obtained by minimizing the negative logarithm of the likelihood function[6–8]

$$J(\boldsymbol{\Theta}) = \frac{1}{2} \sum_{k=1}^{N} [\boldsymbol{z}(t_k) - \boldsymbol{y}(t_k)]^T R^{-1} [\boldsymbol{z}(t_k) - \boldsymbol{y}(t_k)] + \frac{N}{2} \ell n |R| \tag{10}$$

where R is the covariance matrix of the residuals. When started from suitably specified initial values, the, estimates are iteratively updated using the Gauss–Newton or bounded–variable Gauss–Newton method in which the optimization is carried out subject to the specified upper and lower bounds on parameters.[18]

Note that simultaneous estimation of time delays as unknown parameters leads necessarily to a nonlinear model. As already explained, the unknown time delays are estimated through delay matrices; this approach is found to be most efficient. Yet another way to account for delays is through an approximation by a first-order lag, which is simpler but requires additional differential equations and may introduce some dynamic effects, albeit small.[16]

Analysis Techniques and Results

For demonstration purposes, Fig. 8 shows the reconstructed angle of attack and angle of sideslip for just two maneuvers, estimating only the sensitivity factors and biases as shown in Eq. (4), that is, neglecting the time delays. An expanded timescale plot is also shown for a portion of the maneuver, from which it is clearly observed that the measured signal shown by the continuous line lags that estimated shown by dashed lines. On the other hand, accounting for time delays according to Eq. (5) leads to a match shown in Fig. 9

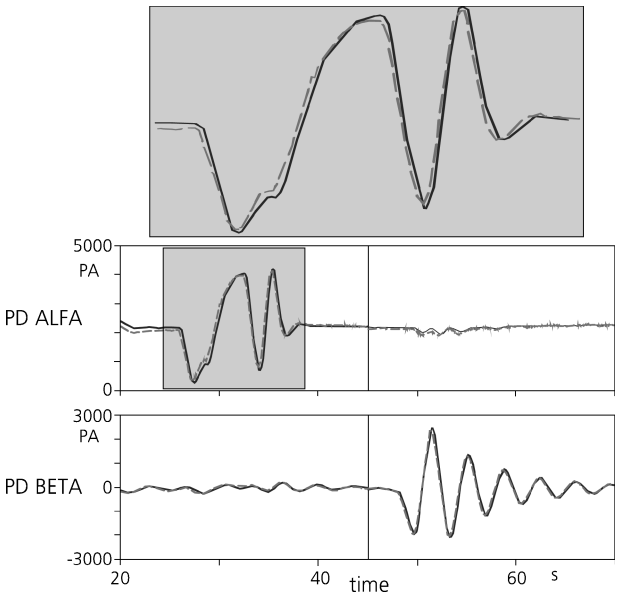

Fig. 8 Estimated flow angles neglecting time delays.

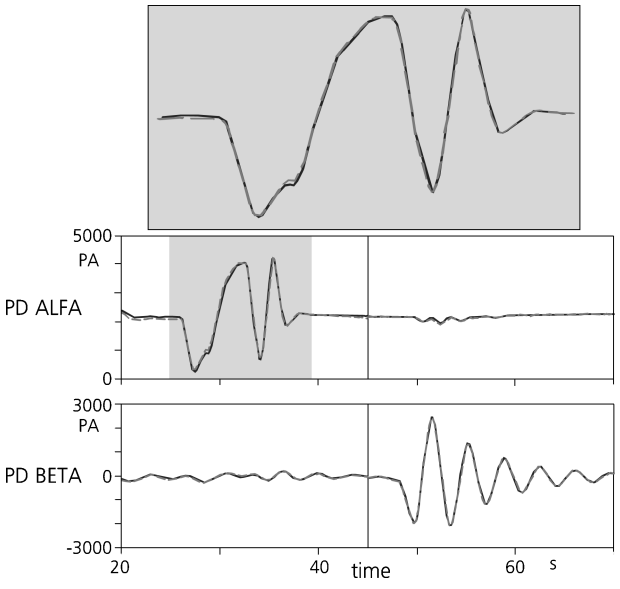

Fig. 9 Estimation accounting for time delays.

and shows significantly improved time synchronization. Repeated analysis of several flight maneuvers at different trim conditions led to consistent values for the time lag. To summarize, both the flow angles showed time delays of the order of 130 ms. From a separate laboratory calibration, it is verified that the identified time delay is mostly due to data recording and preprocessing, but not plastic tubing. The laboratory calibration consisted of applying the known pressures and recording the outputs of the five-hole probes, and it showed a time delay of 120 ms.

The output error method is successively applied to estimate the sensitivity factor and time delays in Eqs. (4) and (5). Figure 10 shows an overview of the data analyzed to calibrate the flow angles. A total of 32 maneuvers are analyzed simultaneously, vertical lines in Fig. 10 mark the different time segments. From Fig. 10e, note that the Mach number covered in the evaluation ranges from 0.25 to about 0.55. The match between the flight measured data (continuous lines) and that reconstructed (dashed lines) is good for all of the variables; Figs. 10a and 10b represent the difference pressures for the angle of attack and angle of sideslip, respectively. In the present case, for the Mach numbers tested, the sensitivity factor being not dependent on the Mach number, it would have been possible to calibrate the flow angle using less data. The trial runs showed that any combination of flight maneuvers yielded comparable and repeatable results. In general, the amount of data needed will depend on the nonlinearity in the sensitivity factor.

Figure 11 shows the flight-path reconstruction results for steady-state sideslip maneuvers. The estimated flow angles match well with the measured variables. The angle of sideslip during these maneuvers ranged from 0 to roughly ± 5 to ± 10 deg.

The analysis of flight maneuvers for Mach 0.6 was carried out separately mainly because, from a priori knowledge, the sensitivity factor is expected to vary with speed. Parameter estimation from flight data confirmed this, however, only for the angle of attack. Time history plots for this case are not shown here because the overall match was qualitatively very good.

Figure 12 shows a comparison of the sensitivity factors estiamted separately from maneuvers at different Mach numbers. To summarize, the estimated sensitivity factors for the angle of attack and angle of sideslip are 0.0819 for Mach variation up to 0.55 compared to 0.079 specified by the manufacturer. For Mach 0.6, the sensitivity factor for angle of attack is estimated to be 0.0781, and for angle of sideslip no Mach dependency could be estimated. Thus, overall,

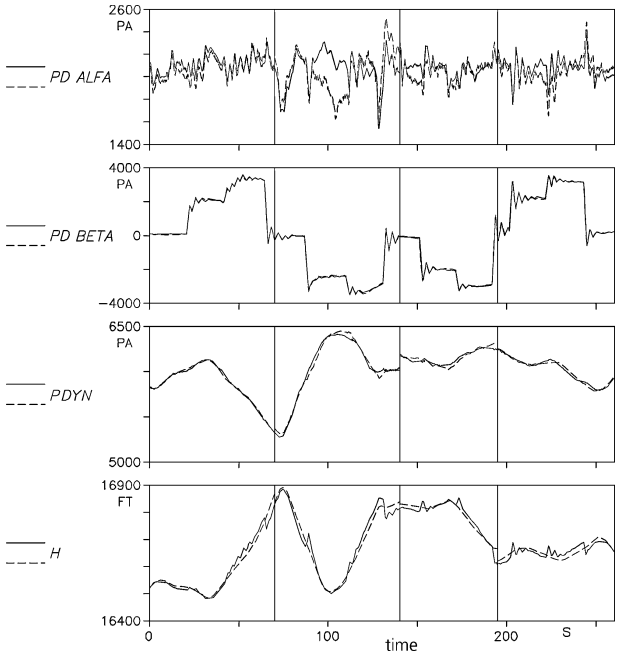

Fig. 11 Curve fits from flight-path reconstruction, steady-state sideslip maneuvers.

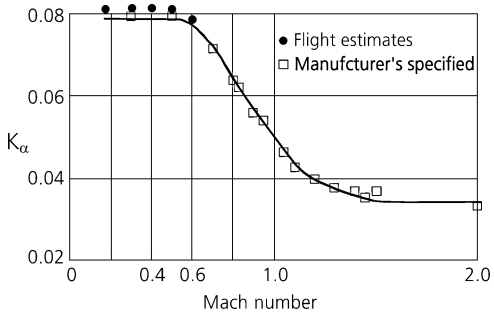

Fig. 12 Comparison of estimated scale factors with manufacturer's data.

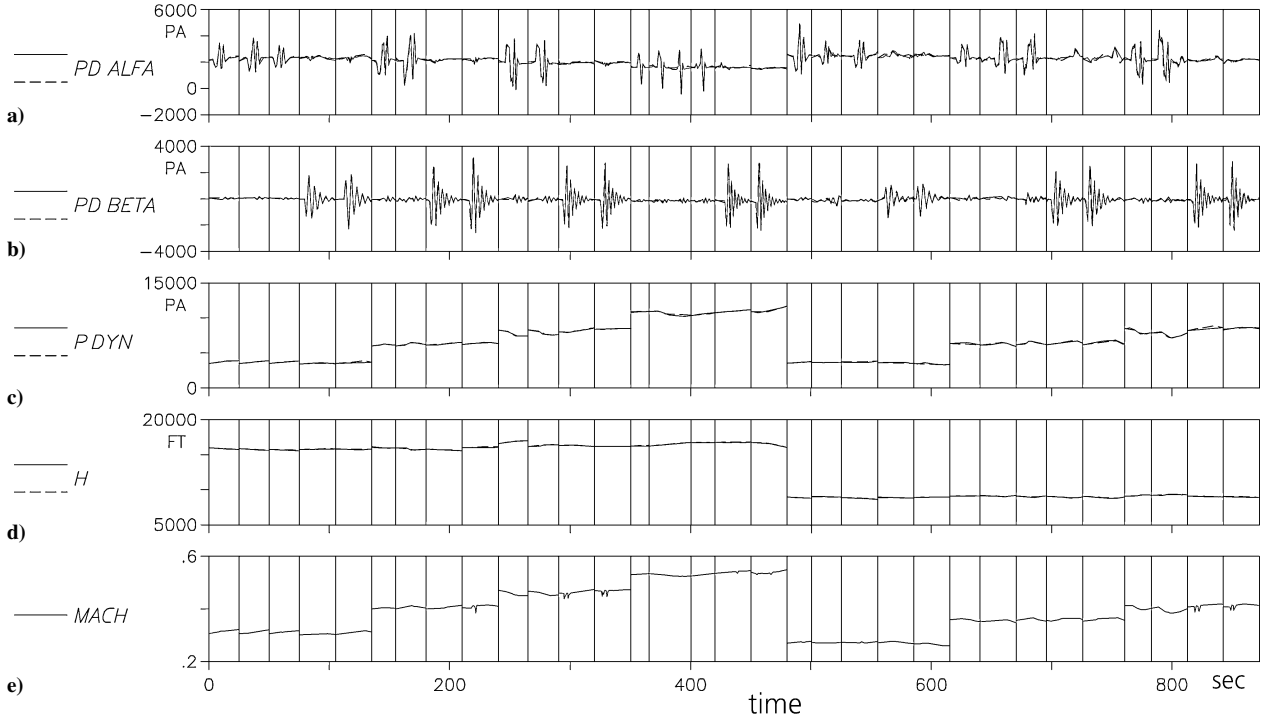

Fig. 10 Curve fits from flight path reconstruction, multiple run analysis: ——, flight measured and - - - -, estimated.

the calibration coefficients obtained from the flight tests agree fairly well with the manufacturer specifications. The measurement of difference pressure for angle attack showed a bias of 131 Pa, whereas that for the angle of sideslip 200 Pa. As already demonstrated, the time delay in both the measurements was of the order of 130 ms. It is, however, necessary to point out that the sensitivity factors, biases, and time delays are system installation specific. Any generalization to other configurations requires careful consideration.

Kalman Filter Technique

A special flight-test procedure, called a wind-box maneuver, and a Kalman filter algorithm incorporating GPS information was proposed and used at the National Research Council, Canada to calibrate a flush air data system, consisting of five pressure ports.[19,20] Calibration of flow angles from such a flush air data system is, in general, configuration and flight condition dependent because the flow at the aircraft nose is strongly distorted. Although in the present investigation the flow angles are not measured by a flush air data system, but rather by a five-hole probe mounted on a noseboom, it is of interest to compare the standard technique described in the preceding section and the approach presented in this section.

The wind-box maneuver leads to a typical horizontal flight track shown in Fig. 13. It consists of acceleration and deceleration phases leading to angle-of-attack variations, build up of steady-state sideslips in both directions, and 90-deg turns to traverse the spatial field in both x and y directions. Typical duration of such a maneuver is about 700 s. Flight tests with ATTAS included two wind-box maneuvers, one at 8000 ft and other at 16,000 ft.

Such wind-box maneuvers are analyzed applying Kalman filter techniques and by incorporating GPS information. The detailed equations for Kalman filter algorithm and those for aircraft velocity components are omitted here for brevity; they are exactly the same as in Ref. 20. The dynamic pressure is modeled as

$$p_{\text{dyn}} = C_{p0} + (1 + C_{p1})p_{\text{dyn\_}m} \tag{11}$$

where C_{p0} and C_{p1} are the unknown coefficients modeling the position error. The flow angles are modeled as

$$\alpha = C_{A0} + C_{A1}(p_{d\alpha}/p_{\text{dyn}}), \qquad \beta = C_{B0} + C_{B1}(p_{d\beta}/p_{\text{dyn}}) \tag{12}$$

where C_{A0} and C_{B0} account for the misalignment between noseboom and aircraft axes, and C_{A1} and C_{B1} are sensitivity factors. As elaborated earlier, $p_{d\alpha}$ and $p_{d\beta}$ are the difference pressures corresponding to angle of attack and angle of sideslip, and p_{dyn} is the dynamic pressure.

The Kalman filter algorithm consists of 18 error states (3 air navigator position errors, 3 wind component errors, 2 calibration errors for angle of attack, 2 calibration errors for angle of sideslip, 2 calibration errors for position error correction, 3 aircraft Euler angle errors, and 3 GPS position offset errors). All of the error states, other than the three air data navigational position errors, are modeled as first-order Gauss–Markov processes. A schematic of the error feedback Kalman filter is shown in Fig. 14.

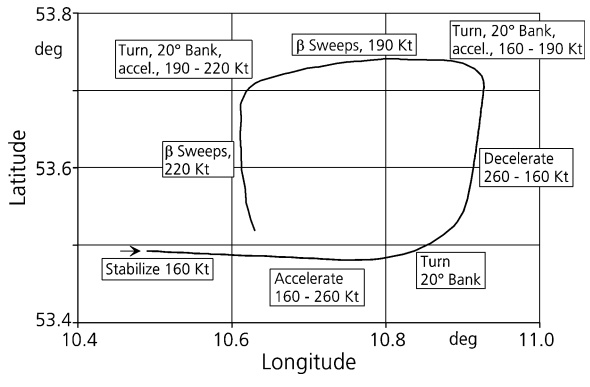

Fig. 13 Typical flight track during wind-box maneuver.

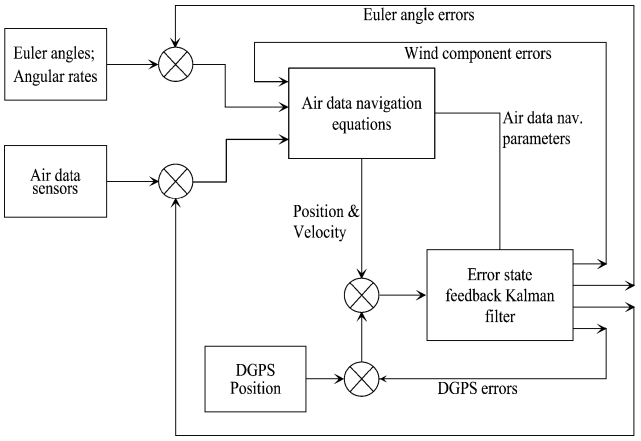

Fig. 14 Schematic of error feedback Kalman filter for calibration of air data system.

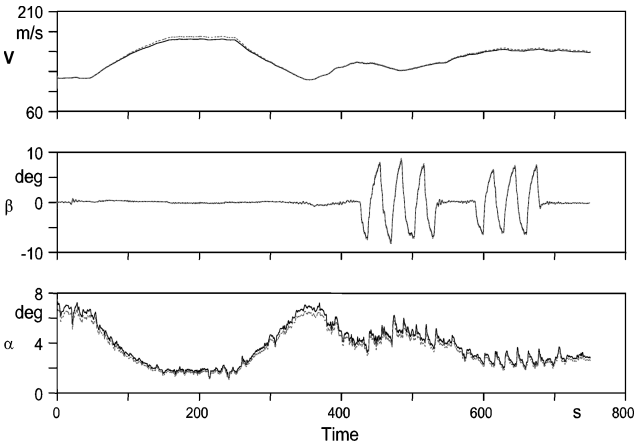

Fig. 15 Flight measured and reconstructed time histories for a wind-box maneuver.

For a typical wind-box maneuver, Fig. 15 shows time histories of the measured and estimated variables. The reconstructed variables match fairly well with the measured data. It is observed that the sensitivity coefficients are estimated with very low standard deviation. The sensitivity coefficients C_{A1} and C_{B1} are estimated as 12.03 and 12.02, respectively.

The results obtained from Eq. (12) applying the Kalman filter techniques to wind-box maneuver are compared with those obtained from Eqs. (4) and (5) applying the output error method to dynamic maneuvers. Although the two sets of equations may appear to be formulated differently, they are basically the same. It is obvious that C_{A1} and C_{B1} appearing in Eq. (12) are inverses of the sensitivity coefficients K_α and K_β appearing in Eq. (4). Thus, the inverse of C_{A1} estimate from wind-box for angle of attack yields 0.0831 ($= 1/12.03$), which compares fairly well with the estimate of K_α ($= 0.0819$). The same is true for the sensitivity factors pertaining to angle of sideslip. The minor differences are attributed primarily to the fact that in the Kalman filter technique the time delays in flow angles were not accounted for. Investigations in the past have demonstrated that omission of time delays can affect estimation results to some extent.[17] Furthermore, the noise covariances were prespecified and kept fixed; tuning of noise covariances can somewhat influence the estimates. Nevertheless, the agreement between the two different analysis techniques applied to two different types of flight maneuvers is good and increases the confidence in the results generated from flight data analysis. Inclusion of time delay in Kalman filter algorithm, although feasible, calls for significant changes in the estimation software. This effort was not made

because the output error is simpler to use and already had the option of estimating the time delays.

Conclusions

A flight-path reconstruction technique is applied to dynamic flight maneuvers to calibrate the angle of attack and angle of sideslip from a five-hole probe. The flight-validated sensitivity coefficients, biases, and time delays in the recorded parameters are determined by the application of the output error method of parameter estimation. Some small deviations in the estimated sensitivity coefficients of the flow angles compared to the manufacturer's data are attributed to location errors. The estimated time delays were reconfirmed through laboratory postverification. In addition, a Kalman filter technique incorporating GPS data is applied to specially flown wind-box maneuvers to calibrate the same signals. The two different flight-test techniques and analysis approaches provided comparable results. As a precursor to the calibration of flow angles, the tower flyby maneuvers were accurately analyzed through redundant techniques to determine the position error in the measured static pressure. A description of the flight maneuvers and of the data analysis is presented.

References

[1]Hanke, D., Wilhelm, K., and Meyer, H. L., "Development and Applications of In-Flight Simulator for Flying Qualities Research at DFVLR," *Proceedings of the NAECON '86 Symposium on Developing Technologies for Revolutionary Applications*, Lecture No. 117, May 1986.

[2]Jategaonkar, R. V., "Identification of the Aerodynamic Model of the DLR Research Aircraft ATTAS from Flight Test Data," DLR, German Aerospace Center, Rept. DLR-FB 90-40, Brunswick, Germany, July 1990.

[3]Jategaonkar, R. V., "Identification of Actuation System and Aerodynamic Effects of Direct-Lift-Control Flaps," *Journal of Aircraft*, Vol. 30, No. 5, 1993, pp. 636–643.

[4]Evans, R. J., Goodwin, G. C., Feik, R. A., Martin, C., and Lozano-Leal, R., "Aircraft Flight Data Compatibility Checking Using Maximum Likelihood and Extended Kalman Filter Estimation," *Proceedings of the 7th IFAC Symposium on Identification and System Parameter Estimation*, York, United Kingdom, Pergamon Press, Oxford, United Kingdom, 1985, pp. 487–492.

[5]Keskar, D. A., and Klein, V., "Determination of Instrumentation Errors from Measured Data Using Maximum Likelihood Method," AIAA Paper 80-1602, 1980.

[6]Hamel, P. G., and Jategaonkar, R. V., "Evolution of Flight Vehicle System Identification," *Journal of Aircraft*, Vol. 33, No. 1, 1996, pp. 9–28.

[7]Maine, R. E., and Iliff, K. W., "Identification of Dynamic Systems," AG-300, AGARD, Vol. 2, Jan. 1985.

[8]Maine, R. E., and Iliff, K. W., "Identification of Dynamic Systems—Applications to Aircraft. Part 1: The Output Error Approach," AG-300, AGARD, Vol. 3, Pt. 1, Dec. 1986.

[9]DeLeo, R. V., and Hagan, F. W., "Flight Calibration of Aircraft Static Pressure Systems," Federal Aviation Agency Contract FA 64WA-5025, Rept. No. RD-66-3, Rosemount Engineering Co., Minneapolis, MN, Jan. 1966.

[10]Brown, E. N., "Position Error Calibration of a Pressure Survey Aircraft Using a Trailing Cone," National Center for Atmospheric Research, Technical Note NCAR/TN-313+STR, Boulder, CO, July 1988.

[11]Gallagher, G. L., Higgins, L. B., Khinoo, L. A., and Pierce, P. W., "Fixed Wing Performance," Naval Test Pilot School Flight Test Manual, Rept. USNTPS-FTM-No. 108, Sept. 1992.

[12]N. N., "Rosemount Model 858 Flow Angle Sensors," Bulletin 1014, Rosemount Inc., Burnsville, MN, 1988.

[13]De Leo, R. V., and Hagen, F. W., "Aerodynamic Performance of Rosemount Model 858AJ Air Data Sensor," Rosemount, Rept. 8767, Minneapolis, MN, July 1976.

[14]Etkin, B., *Dynamics of Atmospheric Flight*, Wiley, New York, 1972.

[15]McRuer, D., Ashkenas, I., and Graham, D., "Aircraft Dynamics and Automatic Control," Princeton Univ. Press, Princeton, NJ, 1973.

[16]Jategaonkar, R. V., "ESTIMA: A Modular and Integrated Software Tool for Parameter Estimation and Simulation of Dynamic Systems–User's Manual, Version 1.0," DLR, German Aerospace Center, Rept. DLR-IB 111-2001/29, Brunswick, Germany, July 2001.

[17]Plaetschke, E., "A Fortran Program for Maximum Likelihood Parameter Estimation in Nonlinear Retarded Flight Mechanics Systems–User's Manual," DFVLR-Mitt. 86-08, Brunswick, Germany, Feb. 1986.

[18]Jategaonkar, R. V., "Bounded-Variable Gauss–Newton Algorithm for Aircraft Parameter Estimation," *Journal of Aircraft*, Vol. 37, No. 4, 2000, pp. 742–744.

[19]Hui, K., Srinivasan, R., and Baillie, S., "Simultaneous Calibration of Aircraft Position Error and Airflow Angles Using Differential GPS," *Canadian Aeronautics and Space Journal*, Vol. 42, No. 4, Dec. 1996, pp. 185–193.

[20]Leach, B., and Hui, K., "In-Flight Technique for Calibrating Air Data Systems Using Kalman Filtering and Smoothing," AIAA Paper 2001-4260, Aug. 2001.